

Electronic Band gaps and transport properties inside graphene superlattices with one-dimensional periodic squared potentials

Li-Gang Wang^{1,2} and Shi-Yao Zhu^{1,2,3}

¹*Centre of Optical Sciences and Department of Physics,*

The Chinese University of Hong Kong, Shatin, N. T., Hong Kong, China

²*Department of Physics, Zhejiang University, Hangzhou, 310027, China*

³*Department of Physics, Hong Kong Baptist University,*

Kowloon Tong, Hong Kong, China

(Dated: 2010.02.11)

Abstract

The electronic transport properties and band structures for the graphene-based one-dimensional (1D) superlattices with periodic squared potentials are investigated. It is found that a new Dirac point is formed, which is exactly located at the energy which corresponds to the zero (volume) averaged wavenumber inside the 1D periodic potentials. The location of such a new Dirac point is robust against variations in the lattice constants, and it is only dependent on the ratio of potential widths. The zero-averaged wavenumber gap associated with the new Dirac point is insensitive to both the lattice constant and the structural disorder, and the defect mode in the zero-averaged wavenumber gap is weakly dependent on the insident angles of carriers.

PACS numbers: 73.61.Wp, 73.20.At, 73.21.-b

I. INTRODUCTION

Recently, the experimental realization of a stable single layer of carbon atoms densely packed in a honeycomb lattice has aroused considerable interest in study of their electronic properties [1, 2]. Such kind of material is well known as graphene, and the low-energy charge carriers in pristine graphene are formally described by a massless Dirac equation with many unusual properties near the Dirac point where the valence band and conduction band touch each other [1–5], such as the linear energy dispersion, the chiral behaviour, ballistic conduction and unusual quantum Hall effect [3, 6], frequency-dependent conductivity [7], gate-tunable optical transitions [8], and so on.

Most recently, there have been a number of interesting theoretical investigations on the graphene superlattices with periodic potential or barrier structures, which can be generated by different methods such as electrostatic potentials [9–12] and magnetic barriers [13–16]. Sometimes periodic arrays of corrugations [17, 18] have also been proposed as graphene superlattices. It is well known that the superlattices are very successful in controlling the electronic structures of many conventional semiconducting materials (e.g. see Ref. [19]). In graphene-based superlattices, researchers have found that a one-dimensional (1D) periodic-potential superlattice may result in the strong anisotropy for the low-energy charge carriers' group velocities that are reduced to zero in one direction but are unchanged in another [10]. Furthermore, Brey and Fertig [20] have shown that such behavior of the anisotropy is a precursor to the formation of further Dirac points in the electronic band structures and new zero energy states are controlled by the parameters of the periodic potentials. Meanwhile, Park *et al.* [21] pointed out that new massless Dirac fermions, which are absent in pristine graphene, could be generated when a slowly varying periodic potential is applied to graphene; and they further found the unusual properties of Landau levels and the quantum Hall effect near these new Dirac fermions, which are adjustable by the superlattice potential parameters [22]. Finally it should also be mentioned that the electronic transmission and conductance through a graphene-based Kronig-Penney potential have been recently studied [23] and the tunable band gap could be obtained in graphene with a noncentrosymmetric superlattice potential [24].

Graphene superlattices are not only of theoretical interest, but also have been experimentally realized. For example, superlattice patterns with periodicity as small as 5 nm have

been imprinted on graphene using the electron-beam induced deposition [25]. Epitaxially grown graphenes on metal (ruthenium or iridium) surfaces [26–32] also show superlattice patterns with several nanometers (about 3 nm to 10 nm) lattice period. Fabrication of periodically patterned gate electrodes is another possible way of making the graphene-based superlattices.

Motivated by these studies, in this paper, we will consider the robust properties of the electronic bandgap structures and transport properties for the graphene under the external periodic potentials by applying appropriate gate voltages. Following the previous work [11], we evaluate the effects of the lattice constants, the angles of the incident charge carriers, the structural disorders and the defect potentials on the properties of electronic band structures and transmissions. It is found that a new Dirac point is exactly located at the energy with the zero (volume) averaged wavenumber inside the 1D periodic potentials, and the location of such a new Dirac point is not dependent on lattice constants but dependent on the ratio of potential widths; and the position of the associated zero-averaged wavenumber gap near the new Dirac point is not only independent of lattice constants but is also weakly dependent on the incident angles. With the increasing of the lattice constants, the zero-averaged wavenumber gap will open and close oscillationally but the center position of this gap does not depend on the lattice constants. Furthermore it is shown that the zero-averaged wavenumber gap is insensitive to the structural disorder, while the other opened gaps in 1D periodic potentials are highly sensitive to the structural disorder. Finally we also find that the defect mode inside the zero-averaged wavenumber gap is weakly dependent on the incident angles while the defect mode in other gaps are highly dependent on the incident angles.

The outline of this paper is the following. In Sec. II, with the help of the additional two-component basis, we introduce a new transfer matrix method, which is different from that in Ref. [11], to calculate the reflection, transmission, and the evolution of the wave function; our transfer matrix method is very useful to deal with the periodic- or multi-squared potentials. In Sec. III, the various effects of the lattice constants, the incident angles of carriers, and the structural disorders on the electronic band structures are discussed in detail; furthermore the transport properties of the defect mode inside the zero-averaged wavenumber gap are also discussed. Finally, in Sec. IV, we summarize our results and draw our conclusions.

II. TRANSFER MATRIX METHOD FOR THE STRUCTURES OF PERIODIC POTENTIALS IN THE MONO-LAYER GRAPHENE

The Hamiltonian of an electron moving inside a mono-layer graphene in the presence of the electrostatic potential $V(x)$, which only depends on the coordinate x , is given by

$$\hat{H} = v_F \boldsymbol{\sigma} \cdot \mathbf{p} + V(x) \hat{I}, \quad (1)$$

where $\mathbf{p} = (p_x, p_y) = (-i\hbar \frac{\partial}{\partial x}, -i\hbar \frac{\partial}{\partial y})$ is the momentum operator with two components, $\boldsymbol{\sigma} = (\sigma_x, \sigma_y)$, and σ_x, σ_y are pauli matrices of the pseudospin, \hat{I} is a 2×2 unit matrix, and $v_F \approx 10^6 \text{m/s}$ is the Fermi velocity. This Hamiltonian acts on a state expressed by a two-component pseudospinor $\Psi = (\tilde{\psi}_A, \tilde{\psi}_B)^T$, where $\tilde{\psi}_A$ and $\tilde{\psi}_B$ are the smooth enveloping functions for two triangular sublattices in graphene. Due to the translation invariance in the y direction, the wave functions $\tilde{\psi}_{A,B}(x, y)$ can be written as $\tilde{\psi}_{A,B}(x, y) = \psi_{A,B}(x) e^{ik_y y}$. Therefore, from Eq. (1), we obtain

$$\frac{d\psi_A}{dx} - k_y \psi_A = ik \psi_B, \quad (2)$$

$$\frac{d\psi_B}{dx} + k_y \psi_B = ik \psi_A, \quad (3)$$

where $k = [E - V(x)]/\hbar v_F$ is the wavevector inside the potential $V(x)$, E is the incident energy of a charge carrier, and $k_0 = E/\hbar v_F$ corresponds to the incident wavevector. Obviously, when $E < V(x)$, the wavevector inside the barrier is opposite to the direction of the electron's velocity. This property leads to a Veselago lens in graphene $p-n$ junctions, which has been predicted by Cheianov, Fal'Ko and Altshuler [33].

In what follows, we assume that the potential $V(x)$ is comprised of periodic structures of squared potentials as shown in Fig. 1. Inside the j th potential, $V_j(x)$ is a constant, therefore, from Eqs. (2) and (3), we can obtain

$$\frac{d^2\psi_A}{dx^2} + (k_j^2 - k_y^2)\psi_A = 0, \quad (4)$$

$$\frac{d^2\psi_B}{dx^2} + (k_j^2 - k_y^2)\psi_B = 0. \quad (5)$$

Here the subscript "j" denotes the quantities in the j th potential. The solutions of Eqs. (4) and (5) are the following forms

$$\psi_A(x) = ae^{iq_j x} + be^{-iq_j x}, \quad (6)$$

$$\psi_B(x) = ce^{iq_j x} + de^{-iq_j x}, \quad (7)$$

where $q_j = \text{sign}(k_j) \sqrt{k_j^2 - k_y^2}$ is the x component of the wavevector inside the j th potential V_j for $k_j^2 > k_y^2$, otherwise $q_j = i \sqrt{k_y^2 - k_j^2}$; and a (c) and b (d) are the amplitudes of the forward and backward propagating spinor components. Substituting Eqs. (6) and (7) into Eqs. (2) and (3), we can find the relations

$$c = \frac{ik_j}{iq_j + k_y} a, \quad (8)$$

$$d = -\frac{ik_j}{iq_j - k_y} b. \quad (9)$$

Using Eqs. (8) and (9), we may obtain

$$\psi_A(x) = ae^{iq_j x} + be^{-iq_j x}, \quad (10)$$

$$\psi_B(x) = a \frac{ik_j}{iq_j + k_y} e^{iq_j x} - b \frac{ik_j}{iq_j - k_y} e^{-iq_j x}. \quad (11)$$

In order to derive the connection for the wave functions $\psi_{A,B}(x)$ between any two positions x_{j-1} and $x_{j-1} + \Delta x$ in the j th potential, we assume a basis $\Phi(x) = \begin{pmatrix} \phi_1(x) \\ \phi_2(x) \end{pmatrix}$, which are expressed as,

$$\phi_1(x) = ae^{iq_j x} + be^{-iq_j x}, \quad (12)$$

$$\phi_2(x) = ae^{iq_j x} - be^{-iq_j x}. \quad (13)$$

Using the above basis, we can re-write Eqs. (10) and (11) as the following form:

$$\begin{pmatrix} \psi_A(x) \\ \psi_B(x) \end{pmatrix} = R_j(E, k_y) \begin{pmatrix} \phi_1(x) \\ \phi_2(x) \end{pmatrix}, \quad (14)$$

where

$$R_j(E, k_y) = \begin{pmatrix} 1 & 0 \\ i \sin \theta_j & \cos \theta_j \end{pmatrix}. \quad (15)$$

Here $\theta_j = \arcsin(k_y/k_j)$ is the angle between two components q_j and k_y in the j th potential. Inside the same potential, from the positions x_{j-1} to $x_{j-1} + \Delta x$, the wavefunction $\begin{pmatrix} \psi_A(x_{j-1}) \\ \psi_B(x_{j-1}) \end{pmatrix}$ evolves into another form $\begin{pmatrix} \psi_A(x_{j-1} + \Delta x) \\ \psi_B(x_{j-1} + \Delta x) \end{pmatrix}$, which can be also expressed in terms of the above basis $\Phi(x)$,

$$\begin{pmatrix} \psi_A(x_{j-1} + \Delta x) \\ \psi_B(x_{j-1} + \Delta x) \end{pmatrix} = T_j(\Delta x, E, k_y) \begin{pmatrix} \phi_1(x_{j-1}) \\ \phi_2(x_{j-1}) \end{pmatrix}, \quad (16)$$

where

$$T_j(\Delta x, E, k_y) = \begin{pmatrix} \cos(q_j \Delta x) & i \sin(q_j \Delta x) \\ i \sin(q_j \Delta x + \theta_j) & \cos(q_j \Delta x + \theta_j) \end{pmatrix}. \quad (17)$$

Therefore, the relation between $\begin{pmatrix} \psi_A(x_{j-1}) \\ \psi_B(x_{j-1}) \end{pmatrix}$ and $\begin{pmatrix} \psi_A(x_{j-1}+\Delta x) \\ \psi_B(x_{j-1}+\Delta x) \end{pmatrix}$ can be finally written as:

$$\begin{pmatrix} \psi_A(x_{j-1} + \Delta x) \\ \psi_B(x_{j-1} + \Delta x) \end{pmatrix} = M_j(\Delta x, E, k_y) \begin{pmatrix} \psi_A(x_{j-1}) \\ \psi_B(x_{j-1}) \end{pmatrix}, \quad (18)$$

where the matrix M_j is given by

$$\begin{aligned} M_j(\Delta x, E, k_y) &= T_j(\Delta x, E, k_y) R_j^{-1}(E, k_y) \\ &= \begin{pmatrix} \frac{\cos(q_j \Delta x - \theta_j)}{\cos \theta_j} & i \frac{\sin(q_j \Delta x)}{\cos \theta_j} \\ i \frac{\sin(q_j \Delta x)}{\cos \theta_j} & \frac{\cos(q_j \Delta x + \theta_j)}{\cos \theta_j} \end{pmatrix}. \end{aligned} \quad (19)$$

It is easily to verify the equality: $\det[M_j] = 1$. Here we would like to point out that in the case of $E = V_j$, the transfer matrix (19) should be recalculated with the similar method and it is given by

$$M_j(\Delta x, E, k_y) = \begin{pmatrix} \exp(k_y \Delta x) & 0 \\ 0 & \exp(-k_y \Delta x) \end{pmatrix}. \quad (20)$$

Meanwhile, in the j th potential ($x_{j-1} < x < x_j$), the wave functions $\psi_{A,B}(x)$ can be also related with $\psi_{A,B}(x_0)$ by

$$\begin{pmatrix} \psi_A(x) \\ \psi_B(x) \end{pmatrix} = Q(\Delta x_j, E, k_y) \begin{pmatrix} \psi_A(x_0) \\ \psi_B(x_0) \end{pmatrix}, \quad (21)$$

where $\Delta x_j = x - x_{j-1}$, $\psi_{A,B}(x_0)$ are wave functions at the incident end of the whole structure, and the matrix Q is given by

$$Q(\Delta x_j, E, k_y) = M_j(\Delta x_j, E, k_y) \prod_{i=1}^{j-1} M_i(w_i, E, k_y). \quad (22)$$

Here w_i is the width of the i th potential, and the matrix Q is related to the transformation of the charge particle's transport in the x direction. Thus we can know the wave functions $\psi_{A,B}(x)$ at any position x inside each potential with the help of a transfer matrix. The initial two-component wave function $\begin{pmatrix} \psi_A(x_0) \\ \psi_B(x_0) \end{pmatrix}$ can be determined by matching the boundary condition. As shown in Fig. 1, we assume that a free electron of energy E is incident from the region $x < 0$ at any incident angle. In this region, the electronic wave function is a superposition of the incident and reflective wavepackets, so at the incident end ($x = 0$), we have the functions $\psi_A(0)$ and $\psi_B(0)$ as follows:

$$\begin{aligned} \psi_A(0) &= \psi_i(E, k_y) + \psi_r(E, k_y) \\ &= (1 + r)\psi_i(E, k_y), \end{aligned} \quad (23)$$

where $\psi_i(E, k_y)$ is the incident wavepacket of the electron at $x = 0$. In order to obtain the function $\psi_B(0)$ at the incident end, from Eqs. (12) and (13), we can re-write the two-component basis in terms of the incident wavepacket, which are given by

$$\phi_1(0) = \psi_i(E, k_y) + \psi_r(E, k_y) = (1 + r)\psi_i(E, k_y), \quad (24)$$

$$\phi_2(0) = \psi_i(E, k_y) - \psi_r(E, k_y) = (1 - r)\psi_i(E, k_x). \quad (25)$$

Therefore, using the relation of Eq. (14), we obtain

$$\begin{aligned} \psi_B(0) &= i \sin \theta_0 \phi_1(0) + \cos \theta_0 \phi_2(0), \\ &= (e^{i\theta_0} - r e^{-i\theta_0}) \psi_i(E, k_y), \end{aligned} \quad (26)$$

where θ_0 is the incident angle of the electron inside the incident region ($x < 0$). In the above derivations, we have used the relation $\psi_r(E, k_y) = r\psi_i(E, k_y)$, where r is the reflection coefficient. Obviously, we have

$$\begin{pmatrix} \psi_A(0) \\ \psi_B(0) \end{pmatrix} = \begin{pmatrix} 1 + r \\ (e^{i\theta_0} - r e^{-i\theta_0}) \end{pmatrix} \psi_i(E, k_y). \quad (27)$$

In the similar way, at the exit end we have

$$\begin{pmatrix} \psi_A(x_e) \\ \psi_B(x_e) \end{pmatrix} = \begin{pmatrix} t \\ t e^{i\theta_e} \end{pmatrix} \psi_i(E, k_y), \quad (28)$$

with the assumption of $\psi_A(x_e) = t\psi_i(E, k_y)$, where t is the transmission coefficient of the electronic wave function through the whole structure, and θ_e is the exit angle at the exit end. Suppose that the matrix \mathbf{X} connects the electronic wave function at the input end with Eq. (27) and that at the exit end with (28), so that we can connect the input and output wave functions by the following equation

$$\begin{pmatrix} \psi_A(x_e) \\ \psi_B(x_e) \end{pmatrix} = \mathbf{X} \begin{pmatrix} \psi_A(0) \\ \psi_B(0) \end{pmatrix}, \quad (29)$$

with

$$\mathbf{X} = \begin{pmatrix} x_{11} & x_{12} \\ x_{21} & x_{22} \end{pmatrix} = \prod_{j=1}^N M_j(w_j, E, k_y). \quad (30)$$

By substituting Eqs. (27,28) into Eq. (29), we have the following relations

$$t = (1 + r)x_{11} + (e^{i\theta_0} - r e^{-i\theta_0})x_{12}, \quad (31)$$

$$t e^{i\theta_e} = (1 + r)x_{21} + (e^{i\theta_0} - r e^{-i\theta_0})x_{22}. \quad (32)$$

Solving the above two equations, we find the reflection and transmission coefficients given by

$$r(E, k_y) = \frac{(x_{22}e^{i\theta_0} - x_{11}e^{i\theta_e}) - x_{12}e^{i(\theta_e+\theta_0)} + x_{21}}{(x_{22}e^{-i\theta_0} + x_{11}e^{i\theta_e}) - x_{12}e^{i(\theta_e-\theta_0)} - x_{21}}, \quad (33)$$

$$t(E, k_y) = \frac{2 \cos \theta_0}{(x_{22}e^{-i\theta_0} + x_{11}e^{i\theta_e}) - x_{12}e^{i(\theta_e-\theta_0)} - x_{21}}, \quad (34)$$

where we have used the property of $\det[\mathbf{X}] = 1$. With Eqs. (21), (23) and (26), now we are able to calculate the two components of the electronic wave function at any position as follows

$$\psi_A(x) = \psi_i(E, k_y) [(1+r) Q_{11} + (e^{i\theta_0} - re^{-i\theta_0})Q_{12}], \quad (35)$$

$$\psi_B(x) = \psi_i(E, k_y) [(1+r) Q_{21} + (e^{i\theta_0} - re^{-i\theta_0})Q_{22}], \quad (36)$$

where Q_{mn} are elements of matrix Q . When we consider the translation of the electron in the y direction for obtaining the wave functions $\tilde{\psi}_{A,B}(x, y)$, the above functions $\psi_{A,B}(x)$ have to be producted by the factor, $Y(y, k_y) = \exp(ik_y \Delta y_j) \prod_{i=1}^{j-1} \exp(ik_y \Delta y_i)$, where $\Delta y_i = w_i \tan \theta_i$ and $\Delta y_j = \Delta x_j \tan \theta_j$. Therefore we finally get

$$\tilde{\psi}_A(x, y) = \psi_i(E, k_y) Y(y, k_y) [(1+r) Q_{11} + (e^{i\theta_0} - re^{-i\theta_0})Q_{12}], \quad (37)$$

$$\tilde{\psi}_B(x, y) = \psi_i(E, k_y) Y(y, k_y) [(1+r) Q_{21} + (e^{i\theta_0} - re^{-i\theta_0})Q_{22}]. \quad (38)$$

We emphasize that these equations are very useful to fully describe the evolutions of the two-component pseudospinor's wave function inside the potential or barrier structures of graphene when the incident electron's wavepacket $\psi_i(E, k_y)$ is given; and furthermore all these formulae are also suitable for multi-potential structures in graphene, not only for periodic potential structures. In the following discussions, we will discuss the properties of the electronic band structure and transmission for the graphene-based periodic squared potential structures.

III. RESULTS AND DISCUSSIONS

In this section, we would like to discuss some unique properties of the band structures in the graphene-based periodic-potential systems by using the above transfer method. First, let us invetigate the electron's bandgap for an infinite periodic structure $(AB)^N$, where the

periodic number N tends to infinity. The magnitude and width of the potential A (B) are with the electrostatic potential $V_{A(B)}$ and width $w_{A(B)}$, as shown in Fig. 1. According to the Bloch's theorem, the electronic dispersion at any incident angle follows the relation

$$\begin{aligned} 2 \cos[\beta_x D] &= \text{Tr}[M_A M_B] \\ &= 2 \cos[q_A w_A + q_B w_B] + \frac{[2 \cos(\theta_A - \theta_B) - 2]}{\cos \theta_A \cos \theta_B} \sin(q_A w_A) \sin(q_B w_B). \end{aligned} \quad (39)$$

When the incident energy of the electron satisfies $V_B < E < V_A$, we have $\theta_A < 0$, $q_A < 0$, $\theta_B > 0$, and $q_B > 0$ for the propagating modes. Then if $q_A w_A = -q_B w_B$, the above equation (39) becomes

$$\cos[\beta_x D] = 1 + \frac{[1 - \cos(2\theta_A)]}{\cos^2 \theta_A} |\sin(q_A w_A)|^2. \quad (40)$$

This equation indicates that, when $q_A w_A = -q_B w_B \neq m\pi$ and $\theta_A \neq 0$, there is no real solution for β_x , i.e., existing a bandgap; Note this bandgap will be close at normal incident case ($\theta_A = 0$) from Eq. (40). Therefore, the location of the touching point of the bands is exactly given by $q_A w_A = -q_B w_B$ at $\theta_A = 0$, i. e., $k_A w_A = -k_B w_B$ or $(V_A - E)w_A = (E - V_B)w_B$.

Figure 2 shows clearly that a band gap opens exactly at energy $E = 25\text{meV}$ under the inclined incident angles (i.e., $k_y \neq 0$), where the condition $q_A d_A = -q_B d_B \neq m\pi$ is satisfied. At the case of normal incidence ($\theta_A = \theta_B = 0$), the upper and lower bands linearly touch together and form a new double-cone Dirac point. The location of the new Dirac point is governed by the equality: $(V_A - E)w_A = (E - V_B)w_B$. For the graphene-based periodic-barrier structure with $V_A \neq 0$ and $V_B = 0$, the new Dirac point is exactly located at $E = V_A/(1 + w_B/w_A)$. From Fig. 2(a-c), one can also find that the location of the new Dirac point is independent of the lattice constants; and the position of the the opened gap associated with the new Dirac point is not only independent of the lattice constants but also is weakly dependent on the incident angles [also see the transmission curves in Figs. 3a and 3b for the finite structures, for example, $(AB)^{25}$]; while other bandgap structuers are not only dependent on the lattice contants but also strongly dependent on different angles (i. e., different k_y). The properties of the opened gap associated with the new Dirac point are very similar to that in the one-dimensional photonic crystals containing the left-haned materials [34], where the so-called zero (volumn) averaged index gap is independent of the lattice constant but only dependent on the ratio of the thicknesses of the right- and left-handed materials [34]. From Fig. 4, one can also find that the locations of both the new Dirac

point and the opened gap are determined by the ratio value of w_A/w_B for the cases with the fixed heights V_A of the potentials. From the above discussion, we find that the volume-averaged wavenumber at the energy of the new Dirac point is zero, therefore such a opened gap associated with the new Dirac point may be called as the zero-averaged wavenumber gap.

From Figs. 2(a-c) and 5(a-c), one can also noted that the slope of the band edges near the new Dirac point gradually becomes smaller as the lattice constant increases under the fixed ratio w_A/w_B and the fixed potential height, and such phenomena have been pointed out in recent work by Brey and Fertig [20]. Actually, from Eq. (39), we can see that as the values of $q_A w_A$ and $-q_B w_B$ gradually reach the values of $m\pi$ ($m = 1, 2, 3, \dots$), the slope of the band edges near the new Dirac point becomes smaller [see Figs. 2(a-c) and 5(a-c)]; once the condition $q_A w_A = -q_B w_B = m\pi$ is satisfied, the zero-averaged wavenumber gap will be close and a pair of new zero-averaged wavenumber states emerges from $k_y = 0$ [see Fig. 5(c)]. Here we would like to emphasize that the properties of these novel zero-averaged wavenumber states are similar to that of the zero-energy states in the previous work [20]. Figure 5(d) shows how the zero-averaged wavenumber gap does gradually close with the increasing of the lattice constant under the fixed transversal wavenumber $k_y = 0.01\text{nm}^{-1}$ and the fixed ratio w_A/w_B . From Fig. 5(d), one can find that the zero-averaged wavenumber gap is very speical and it is open and close oscillationly with the increasing of the lattice constant, and the center position of the zero-averaged wavenumber gap is also independent of the lattice constant. However, the other opened gaps are largely shifted with the increasing of the lattice constant.

Now we turn to consider the transmission of an electron passing through a finite graphene-based periodic-potential structure, e. g., $(AB)^{30}$, with the width deviation under different incident angles. Figure 6 shows the effect of the structural disorder on electronic transimitivities. Figures 6a, 6b and 6c correspond to the transmissions through the periodic-potential structures with the width deviation (random uniform deviate) of $\pm 2.5\text{nm}$, $\pm 3.75\text{nm}$, and $\pm 5.0\text{nm}$, respectively. From Figs. (6a)-(6c), it is clear that the higher opened gap is destroyed by strong disorder, but the zero-averaged wavenumber gap survives. The robustness of the zero-averaged wavenumber gap comes from the fact that the zero-averaged wavenumber solution remains invariant under disorder that is symmetric (+ and - equally probable). It should be emphasized again that the position of the zero-averaged wavenumber gap near

the new Dirac point is insensitive to both the incident angles and the disorder. [see Fig. 3b and Fig. 6].

Finally, we turn our attention to the effect of a defect potential on the property of the electron's transport inside the zero-averaged wavenumber gap. Here we consider the transmission of an electron passing through a graphene-based periodic potential structure with a defect potential, e. g., $(AB)^{30}D(BA)^{30}$, where the symbol "D" denotes the defect barrier. In Fig. 7(a), it shows the electronic transmittivity through the structure under different incident angles. One can see that there is a defect mode respectively occurring inside the zero-averaged wavenumber gap and the higher bandgap, and the location of the defect mode inside the zero-averaged wavenumber gap is very weakly dependent on the incident angle but the defect mode in the higher bandgap is strongly sensitive to the incident angle. It is clear shown in Fig. 7(b) that the energy of the defect mode inside the zero-averaged wavenumber gap is almost independent of the angles while the location of the defect mode in the higher bandgap has a large shift with the increasing of the incident angle.

IV. CONCLUSIONS

In summary, we studied the electronic band structures and transmission of carriers in the graphene-based 1D periodic squared-potential superlattices. For the 1D periodic squared-potential structure, it is found that a new Dirac point does exactly occurs at the energy that corresponds to the zero (volume) averaged wavenumber inside the system, and the location of such a new Dirac point is independent of lattice constants but dependent on the ratio of potential widths. It is also shown that the location of the zero-averaged wavenumber gap associated with the new Dirac point is not only independent of lattice constants but is also weakly dependent on the incident angles. As the lattice constant increases for the structures with the fixed ratio of potential widths, this zero-averaged wavenumber gap is open and close oscillationally around the energy of the new Dirac point. We further showed the robustness of the zero-averaged wavenumber gap against the structural disorder, which has a sensitive effect on other opened gaps of the system. Finally we saw that the defect mode inside the zero-averaged wavenumber gap is weakly dependent on the insident angles while the defect mode in other gaps are highly dependent on the incident angles. Our analytical and numerical results on the properties of the new Dirac point, the novel band gap structure

and defect mode are hopefully of use to pertinent experiments.

Acknowledgments

This work is supported by RGC 403609 and CUHK 2060360, and partially supported by the National Natural Science Foundation of China (10604047) and HKUST3/06C.

-
- [1] K. S. Novoselov, A. K. Geim, S. V. Morozov, D. Jiang, Y. Zhang, S. V. Dubonos, I. V. Grigorieva, and A. A. Firsov, *Science*, **306**, 666(2004).
 - [2] Y. Zhang, Y. W. Tan, H. L. Stormer, and P. Kim, *Nature (London)* **438**, 201 (2005).
 - [3] K. S. Novoselov, A. K. Geim, S. V. Morozov, D. Jiang, M. I. Katsnelson, I. V. Grigorieva, S. V. Dubonos and A. A. Firsov, *Nature* **438**, 197-200 (2005).
 - [4] M. I. Katsnelson, K. S. Novoselov and A. K. Geim, *Nature Phys.* **2**, 620 (2006).
 - [5] For recent reviews, see A. K. Geim, and K. S. Novoselov, *Nature Mater.* **6**, 183-191 (2007); C. W. J. Beenakker, *Rev. Mod. Phys.* **80**, 1337 (2008); A. H. Castro Neto, F. Guinea, N. M. R. Peres, K. S. Novoselov, and A. K. Geim, *Rev. Mod. Phys.* **81**, 109 (2009).
 - [6] M. S. Purewal, Y. Zhang, and P. Kim, *Phys. Status Solidi B* **243**, 3418 (2006).
 - [7] A. B. Kuzmenko, E. van Heumen, F. Carbone, and D. van der Marel, *Phys. Rev. Lett.* **100**, 117401 (2008).
 - [8] F. Wang, Y. Zhang, C. Tian, C. Girit, A. Zettl, M. Crommie, and Y. R. Shen, *Science* **320**, 206 (2008).
 - [9] C. Bai and X. Zhang, *Phys. Rev. B* **76**, 075430 (2007).
 - [10] C. -H. Park, L. Yang, Y.-W. Son, M. L. Cohen, and S. G. Louie, *Nature Phys.* **4**, 213 (2008).
 - [11] M. Barbier, F. M. Peeters, P. Vasilopoulos, and J. M. Pereira, Jr., *Phys. Rev. B* **77**, 115446 (2008).
 - [12] C.-H. Park, L. Yang, Y.-W. Son, M. L. Cohen, and S. G. Louie, *Phys. Rev. Lett.* **101**, 126804 (2008).
 - [13] M. Ramezani Masir, P. Vasilopoulos, A. Matulis, and F. M. Peeters, *Phys. Rev. B* **77**, 235443 (2008).
 - [14] M. Ramezani Masir, P. Vasilopoulos, and F. M. Peeters, *Phys. Rev. B* **79**, 035409 (2009).

- [15] L. Dell’Anna and A. De Martino, Phys. Rev. B **79**, 045420 (2009); L. Dell’Anna¹ and A. De Martino, Phys. Rev. B **80**, 155416 (2009).
- [16] S. Ghosh and M. Sharma, J. Phys. Condens. Matter **21**, 292204 (2009).
- [17] F. Guinea, M. I. Katsnelson, and M. A. H. Vozmediano, Phys. Rev. B **77**, 075422 (2008).
- [18] A. Isacsson, L. M. Jonsson, J. M. Kinaret, and M. Jonson, Phys. Rev. B **77**, 035423 (2008).
- [19] R. Tsu, *Superlattice to Nanoelectronics* (Elsevier, Oxford, 2005).
- [20] L. Brey and H. A. Fertig, Phys. Rev. Lett. **103**, 046809 (2009).
- [21] C. H. Park, L. Yang, Y. W. Son, M. L. Cohen, and S. G. Louie, Phys. Rev. Lett. **101**, 126804 (2008).
- [22] C. H. Park, Y. W. Son, L. Yang, M. L. Cohen, and S. G. Louie, Phys. Rev. Lett. **103**, 046808 (2009).
- [23] M. Barbier, P. Vasilopoulos, and F. M. Peeters, Phys. Rev. B **80**, 205415 (2009).
- [24] R. P. Tiwari and D. Stroud, Phys. Rev. B. **79**, 205435 (2009).
- [25] J. C. Meyer, C. O. Girit, M. F. Crommie, and A. Zettl, Appl. Phys. Lett. **92**, 123110 (2008).
- [26] S. Marchini, S. Günther, and J. Wintterlin, Phys. Rev. B **76**, 075429(2007).
- [27] A. L. Vázquez de Parga, F. Calleja, B. Borca, M. C. G. Passeggi, Jr., J. J. Hinarejos, F. Guinea, and R. Miranda, Phys. Rev. Lett. **100**, 056807 (2008)
- [28] Y. Pan, H. Zhang, D. Shi, J. Sun, S. Du, F. Liu and H. Gao, Adv. Mater. **20**, 1-4 (2008).
- [29] P. W. Sutter, J. I. Flege, and E. A. Sutter, Nature Mater. **7**, 406 (2008).
- [30] D. Martoccia et al., Phys. Rev. Lett. **101**, 126102 (2008).
- [31] J. Coraux, A. T. N’Diaye, C. Busse, and T. Michely, Nano Lett. **8**, 565 (2008).
- [32] I. Pletikosić, M. Kralj, P. Pervan, R. Brako, J. Coraux, A. T. N’Diaye, C. Busse, and T. Michely, Phys. Rev. Lett. **102**, 056808 (2009).
- [33] V. V. Cheianov, V. Fal’ko, and B. L. Altshuler, Science **315**, 1252 (2007).
- [34] J. Li, L. Zhou, C. T. Chan, and P. Shen, Phys. Rev. Lett. **90**, 083901 (2003).

Figures Captions:

Fig. 1. (a) Schematic representation of the finite periodic squared potential structure in $x - y$ plane. Dark regions denote the electrodes to apply the periodic potentials on the graphene. (b) The profiles of the periodic potentials applied on the monolayer graphene.

Fig. 2. (Color online). Electronic band structures for (a) $w_A = w_B = 20\text{nm}$, (b) $w_A = w_B = 30\text{nm}$ and (c) $w_A = w_B = 40\text{nm}$, with $V_A = 50\text{meV}$ and $V_B = 0$ in all cases. The dashed lines denote the "light cones" of the incident electrons, and the dot line denotes the location of the new Dirac points.

Fig. 3. (Color online). Transmitivities of the finite periodic-potential structure $(AB)^{25}$ under (a) different lattice constants with a fixed ratio $w_A/w_B = 1$ and an incident angle $\theta_0 = 10^\circ$ and (b) different incident angles with the fixed lattice parameters $w_A = w_B = 30\text{nm}$.

Fig. 4. (Color online). Electronic band structures for (a) $w_A/w_B = 1$, (b) $w_A/w_B = 3/2$, and (c) $w_A/w_B = 2$, with $V_A = 50\text{meV}$, $V_B = 0$ and $w_B = 20\text{nm}$ in all cases. The dashed lines denote the locations of the new Dirac points.

Fig. 5. (Color online). Electronic band structures for (a) $w_A = w_B = 60\text{nm}$, (b) $w_A = w_B = 80\text{nm}$ and (c) $w_A = w_B = 100\text{nm}$; and (d) dependence of the bandgap structure on the lattice constant w with a fixed transversal wavenumber $k_y = 0.01\text{nm}^{-1}$ and $w_A = w_B = w$. Other parameters are the same as in Fig. 2.

Fig. 6. (Color online). The effect of the structural disorder on electronic transmittivity $T = |t|^2$ under different incident angles: the solid lines for the incident angle $\theta_0 = 1^\circ$, the dashed lines for $\theta_0 = 5^\circ$, the dashed-dot lines for $\theta_0 = 10^\circ$, and the short-dashed lines for $\theta_0 = 15^\circ$, with $V_A = 50\text{meV}$ and $V_B = 0$, and $w_A = w_B = (20 + R)\text{nm}$, where R is a random number for the case (a) between $+2.5\text{ nm}$ and -2.5 nm , for the case (b) between $+3.75\text{ nm}$ and -3.75 nm , and for the case (c) between $+5\text{ nm}$ and -5 nm .

Fig. 7. (Color online). (a) The transmittivity as a function of the incident electronic energy in a periodic-potential structure with a defect potential D , $(AB)^{30}D(BA)^{30}$. (b) Dependence of the defect modes on the incident angles. The parameters of the defect potential are $w_D = 70\text{nm}$ and $V_D = 50\text{meV}$, and other parameters are $V_A = 50\text{meV}$, $V_B = 0$, and $w_A = w_B = 20\text{nm}$.

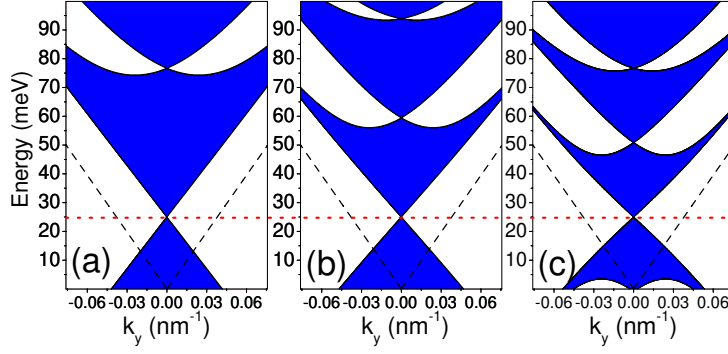


FIG. 2: (Color online) Electronic band structures for (a) $w_A = w_B = 20\text{nm}$, (b) $w_A = w_B = 30\text{nm}$ and (c) $w_A = w_B = 40\text{nm}$, with $V_A = 50\text{meV}$ and $V_B = 0$ in all cases. The dashed lines denote the "light cones" of the incident electrons, and the dot line denotes the location of the new Dirac points.

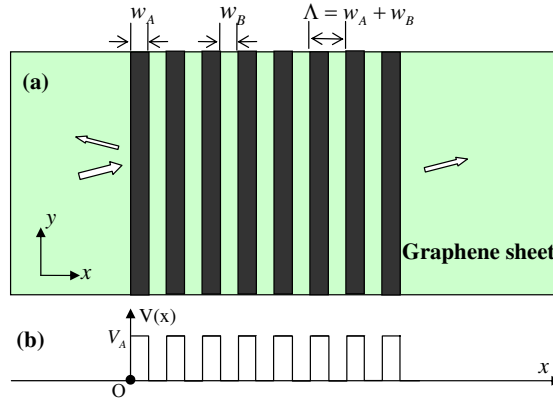


FIG. 1: (Color online) (a) Schematic representation of the finite periodic squared potential structure in $x - y$ plane. Dark regions denote the electrodes to apply the periodic potentials on the graphene. (b) The profiles of the periodic potentials applied on the monolayer graphene.

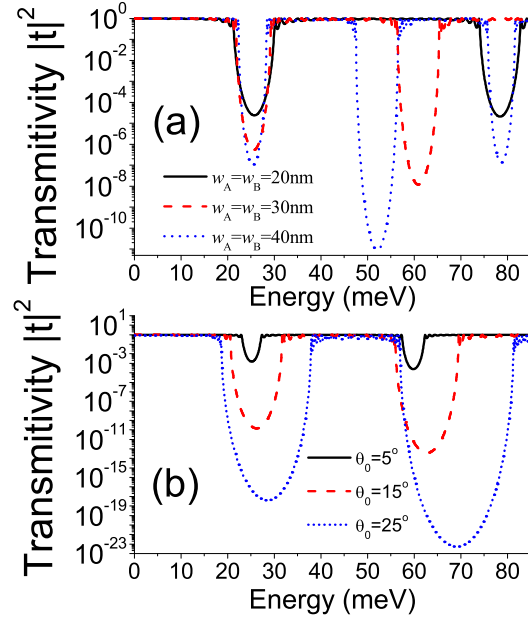


FIG. 3: (Color online) Transmittivities of the finite periodic-potential structure $(AB)^{25}$ under (a) different lattice constants with a fixed ratio $w_A/w_B = 1$ and an incident angle $\theta_0 = 10^\circ$ and (b) different incident angles with the fixed lattice parameters $w_A = w_B = 30\text{nm}$.

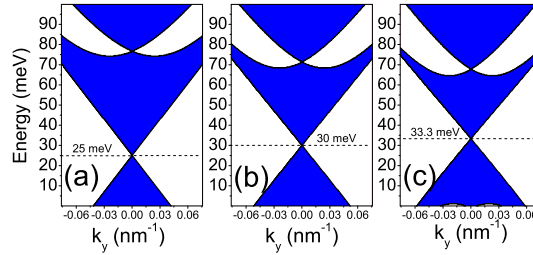


FIG. 4: (Color online) Electronic band structures for (a) $w_A/w_B = 1$, (b) $w_A/w_B = 3/2$, and (c) $w_A/w_B = 2$, with $V_A = 50\text{meV}$, $V_B = 0$ and $w_B = 20\text{nm}$ in all cases. The dashed lines denote the locations of the new Dirac points.

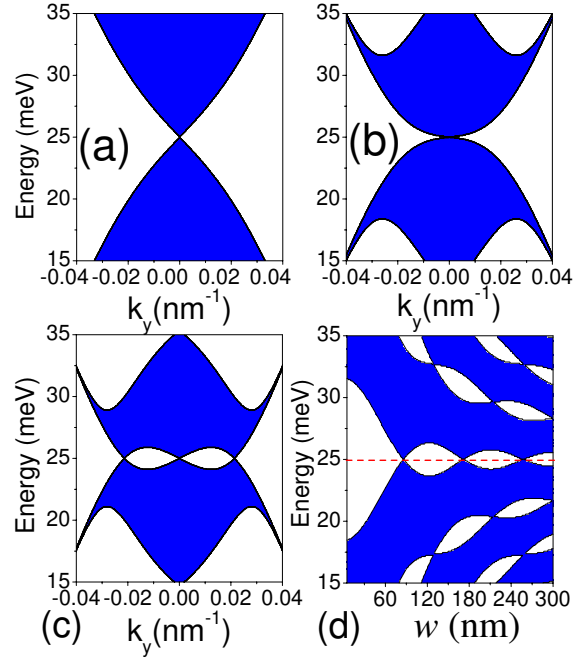


FIG. 5: (Color online) Electronic band structures for (a) $w_A = w_B = 60\text{nm}$, (b) $w_A = w_B = 80\text{nm}$ and (c) $w_A = w_B = 100\text{nm}$; and (d) dependence of the bandgap structure on the lattice constant w with a fixed transversal wavenumber $k_y = 0.01\text{nm}^{-1}$ and $w_A = w_B = w$. Other parameters are the same as in Fig. 2.

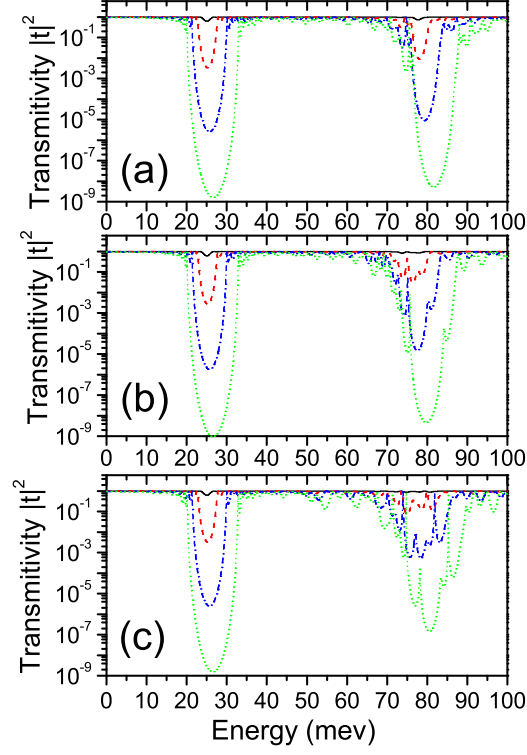


FIG. 6: (Color online) The effect of the structural disorder on electronic transmittivity $T = |t|^2$ under different incident angles: the solid lines for the incident angle $\theta_0 = 1^\circ$, the dashed lines for $\theta_0 = 5^\circ$, the dashed-dot lines for $\theta_0 = 10^\circ$, and the short-dashed lines for $\theta_0 = 15^\circ$, with $V_A = 50\text{meV}$ and $V_B = 0$, and $w_A = w_B = (20 + R)\text{nm}$, where R is a random number for the case (a) between $+2.5\text{ nm}$ and -2.5 nm , for the case (b) between $+3.75\text{ nm}$ and -3.75 nm , and for the case (c) between $+5\text{ nm}$ and -5 nm .

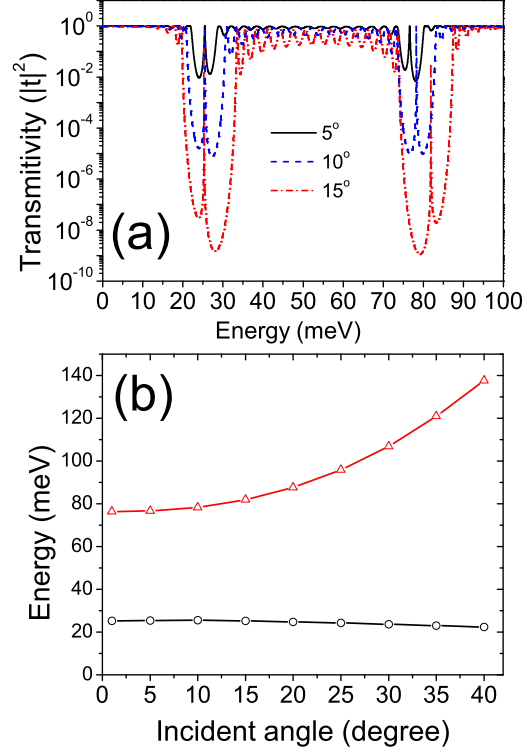


FIG. 7: (Color online) (a) The transmittivity as a function of the incident electronic energy in a periodic-potential structure with a defect potential D , $(AB)^{30}D(BA)^{30}$. (b) Dependence of the defect modes on the incident angles. The parameters of the defect potential are $w_D = 70nm$ and $V_D = 50meV$, and other parameters are $V_A = 50meV$, $V_B = 0$, and $w_A = w_B = 20nm$.